Journal of
Ceramic Science
and Technology

J. Ceram. Sci. Tech., 02 [02] 133-138 (2011)
DOI: 10.4416/JCST2011-00005
available online at: http://www.ceramic-science.com

Residual Stress Strengthening in Layered Tricalcium Phosphate (TCP) Bioceramics

E. Hahn[1], T. Fey*[1], K. Zuo[2], D.-L. Jiang[2], P. Greil[1]

[1]University of Erlangen-Nuremberg, Department of Materials Science (Glass and Ceramics), Erlangen, Germany
[2]Shanghai Institute of Ceramics, State Key Laboratory for Engineering Ceramics, Academy of Sciences, Shanghai, China

received February 4, 2011; received in revised form March 18, 2011; accepted March 19, 2011

Abstract

Residual compressive stress formation on the outer surface layers of bioresorbable calcium phosphate multilayer composites was investigated in order to increase their strength. Multilayer laminates of β-$Ca_3(PO_4)_2$ (TCP) from two different powders were prepared by means of tape casting, laminate pressing, and pressureless sintering. As the laminates cooled from sintering temperature, differences in thermal contraction between the surface layer prepared from a Mg^{2+}-doped β-TCP powder and the core layers caused the generation of surface stresses. The relaxation strain upon removing the surface layer by continuous etching in HNO_3 was measured and the distribution of residual stress near the surface was derived. Compressive stresses of approximately 10 MPa were measured, which offer further potential to improve the load-carrying capability of resorbable TZP bioceramics for application in bone defect and trauma treatment.

Keywords: Calcium phosphate bioceramics, tape-cast laminates, residual stress strengthening

I. Introduction

Calcium phosphate bioceramics based on hydroxyapatite (HAP) $Ca_5(PO_4)_3OH$ and tricalcium phosphate (TCP) β-$Ca_3(PO_4)_2$ are commonly applied for treatment of bone defects [1]. HAP is significantly more stable in the human body whereas TCP can be used as resorbable material. Single-phase as well as biphasic mixtures of HAP and TCP are applied in bone repair as bulk material, as porous structures, in particulate form, in combination with other materials as composites and as coatings [2,3]. Owing to the poor mechanical properties of β-TCP bioceramics (bending strength (hot-pressed) < 125 MPa, Young's modulus < 60 GPa, toughness < 1 MPa·$m^{1/2}$) compared to cortical human bone (strength < 150 MPa; Young's modulus < 30 GPa; toughness < 12 MPa·$m^{1/2}$) [4,5], it has not yet been possible to use implants made of β-TCP in load-bearing contact to bone. Increasing the sintered density by adding sintering aids such as glasses, processing of nanoscale microstructures, and formation of ceramic/polymer composites are among the most promising approaches for improving the mechanical properties of calcium-phosphate-based bioceramics [6–8].

Enhancement of strength as well as toughness by means of macroscopic surface compressive stresses has been successively demonstrated for improvement of the mechanical properties of brittle ceramic materials [9–12]. Probably the most popular examples of application are safety glass and thin display glass sheets. Thermal expansion mismatch, phase transformation, density changes owing to crystallization or ion exchange, and microplasticity induced by contact loading (grinding, shot peening, wear) are relevant mechanisms being used for macroscopic residual stress formation in ceramics. Toughening of layered ceramic composites with residual surface compression has been demonstrated in a variety of engineering ceramic materials systems. For example, an increase of fracture toughness from 5 MPa·$m^{1/2}$ to 8.5 MPa·$m^{1/2}$ was reported in multilayer Si_3N_4/Si_3N_4+TiN ceramics having compressive surface stress values ranging from 130–530 MPa [13]. A residual compression stress of ~400 MPa developed in the outer layers by constrained transformation of unstabilized zirconia from the tetragonal to the monoclinic phase enhanced the apparent fracture toughness to values of 30 MPa·$m^{1/2}$ in a system where the intrinsic fracture toughness was only 5 to 7 MPa·$m^{1/2}$ [11].

While residual stresses in engineering ceramics were primarily considered for enhancement of strength and toughness, reports on residual stresses in calcium phosphate ceramics are mainly focused on HAP coatings on metal substrates. Internal residual stresses in plasma-sprayed HAP coatings on Ti-alloy substrate ranging from tensile (10–25 MPa) [14] to compressive (15–30 MPa) [15] were measured. Significantly higher compressive stresses of 130–275 MPa were reported for sol-gel-derived fluoridated hydroxyapatite coatings on Ti6Al4V substrates [16]. Internal residual stress in the HAP coatings were iden-

* Corresponding author: tobias.fey@ww.uni-erlangen.de

tified as having an important influence on determining the durability of the coated implants. Thus, compressive stresses may weaken the bonding between the coating and substrate [15] and influence the dissolution properties of the HAP coating [17]. Residual stress formation on bulk calcium phosphate ceramics, however, has not yet been explored to our knowledge. This study aims to explore the formation of residual compression stresses on the surface of β-TCP calcium phosphate multilayer laminate composites. Layered composites with various stacking orders were prepared from β-TCP powders with different microstructures. The residual stress was evaluated with the strain relaxation method upon removing the surface layer from one surface. Residual stress formation on layered calcium phosphate ceramics may enable future development of load-bearing bioactive implant materials.

II. Experimental Procedure

(1) β-TCP powders and tape casting

Two commercial β-TCP powders A (β-TCP, Merck KGaG, Darmstadt, D) and B (β-TCP, Fluidinova, Porto, P) were applied for tape processing. The grain size distribution of the powders was measured by means of laser diffraction (Mastersizer 2000, APA 2000 with Hydro 2000S measuring cell; Malvern Instruments, Herrenberg, D). The Brunauer Emmett-Teller method was used (ASAP 2000, Micromeritics, Norcross, USA) to determine the specific surface area of the powders. The two powders differ in their mean particle size (A: 4.3 µm; B: 3.5 µm) and the specific surface area (S_V) (A: 63.4 m^2/g; B 94.5 m^2/g). The discrepancy of mean particle size and crystallite size (d_c) of 30 nm (A) and 20 nm (B) calculated from the specific surface area ($d_c \approx 6/(S_V \varrho)$ with density $\varrho = 3.07\ g/cm^3$) indicates a high degree of agglomeration, which was confirmed in SEM analyses (Quanta 200, FEI, Eindhoven, NL). Furthermore, powder A contained a small amount of stabilizing Mg (0.27 wt%) in order to increase the β to α phase transformation temperature of TCP [18]. The Ca/P ratio determined by ICP spectroscopy (Spectro Fleming Modula, Spectro Analytical Instruments) was 1.4 (A) and 1.5 (B) (theoretical value 1.5). XRD (Kristalloflex D500 equipped with an Anton Paar HTK 10 chamber, Siemens, Karlsruhe, D) working with monochromated $Cu_{K\alpha}$ proved the crystalline phase composition to be single-phase β-TCP (JCPDS 009 – 00169) up to 1300 °C (A) and 1200 °C (B) where phase transformation to α-TCP was detected. Prior to processing of the tape-casting slurries, both powders were calcined at 900 °C for 2 h in order to reduce the specific surface area. Calcination resulted in an increase in crystallite size to approximately 0.4 µm (A) and 0.58 µm (B) whereas the particle size (e.g. the agglomerate size) remained almost constant.

Aqueous slurries containing 37 vol% TCP powder, 29 vol% H_2O, 2 vol% dispersant (Ammonium-Polycarboxylate, Melpers 3440, BASF, Ludwigshafen, D) and 32 vol% binder (Polyvinylacetate dispersion Dolacol B 4014, Zschimmer + Schwarz, Lahnstein, D) were prepared by mixing for 24 h in a shaker mixer (Turbula, Willy A. Bachhofen, Basel, CH) and defoaming in a planetary mixer (Thinky-Mixer ARE-250, Thinky, Tokyo, J). Grain size distributions were measured after mixing (Master Sizer 2000, APA 2000 with Hydro 2000S, Malvern Instruments, Worcestershire, GB). Tapes with a thickness of 130 – 150 µm were prepared with the doctor blade process, the slurry being cast on a silicone-coated polyethylene terephthalate (PET) carrier foil. The laboratory tape-casting device was equipped with two chambers and two blades and a drawing velocity of 700 mm/min was applied.

(2) Lamination and sintering

Green tapes were stacked and laminated (Polystat 200 t, Servitec Maschinenbau GmbH, Wustermark, D), applying a pressure of 40 MPa for 15 min. Rectangular samples measuring 40 mm × 40 mm were prepared by stapling 20 tapes, resulting in a total body thickness of approximately 2.3 – 2.5 mm (shrinkage perpendicular to sheet plane upon laminate pressing ~ 23 %). No additional adhesive was applied to the tapes prior to lamination pressing. The thermoplastic binder present in the tape was selected for its low glass transition temperature of -20 °C to allow cold lamination bonding at 30 °C [19]. Monolithic laminates of 20 tapes were prepared from A and B TCP powders, respectively, and sandwich laminates of 20 B layers covered with one A layer on each side were also formed. This A-B-A laminate structure was selected from the thermal expansion behaviour measured on the two different powder tapes (see results).

The monolithic and the sandwich laminates were sintered at 1150 °C for 2 h in an electrically heated tube furnace in air atmosphere. The thickness of sintered laminate was approximately 2.08 mm with an A surface layer thickness of approximately 0.09 mm and a B core of 1.9 mm (thickness ratio A/B of 0.045). Up to 600 °C, the heating rate was limited to 1 °C/min to facilitate binder burnout. From 600 °C to the final sintering temperature, the heating rate was raised to 3.6 °C/min.

(3) Characterization

Length, width, height, and mass of the green specimens were measured for green density calculation. Sintered density was measured with the Archimedes method. Thermal expansion of the monolithic A and B laminates was measured on rectangular samples (12 mm x 6 mm x 1.9 mm) by means of differential dilatometry (Dil 402 C, Netzsch, Selb, D), applying α-Al_2O_3 for reference. The microstructure of sintered laminates was analyzed from cross-sections perpendicular to the laminate stacking with SEM. Prior to examination, the specimen surface was sputtered with gold.

The modulus of rupture of the multilayered ceramics was measured by biaxial bending loading (Instron 4204, Instron Corp., Canton, MA, USA) using a concentric ring-on-ring gauge geometry (8.2/18 mm in diameter). Samples were loaded as sintered without grinding and polishing and a cross-head velocity of 0.5 mm/min was applied. The fracture stress σ_f was derived from the specimen geometry, the loading geometry and the load applied F_{max} according to [20]

$$\sigma_f = \frac{3F_{max}}{2\pi h^2}\left[2(1-\nu)\frac{r_2^2 - r_1^2}{e\left(1+\sqrt{2}\right)} + (1+\nu)\ln\frac{r_2}{r_1}\right] \quad (1)$$

where, ν is Poisson's ratio ($\nu = 0.25$), r_1 is the radius of the load-ring ($r_1 = 1.5$ mm), r_2 is the radius of the support ring ($r_2 = 4$ mm), e is the edge length of the quadratic samples, and h is the sample height. The reported average (σ_f) is the mean of ten measurements. Young's modulus was derived from ultrasonic velocity measurements (USD 10, Krautkramer, Hürth, D), applying a frequency of > 1 MHz to specimens of same geometry.

(4) Residual stress measurements

The residual stress profile on the surface-near region was derived from measurements of the curvature upon strain relaxation when one of the surface layers was removed by etching in 63 % HNO_3, Fig. 1 [21]. A strain gauge element (LY 61 6/350, HBM, Darmstadt, Germany) recorded the relaxation strain ε relative to a reference sample (covered with an etch-resistant coating) to compensate for the temperature drift during the measurement. Applying Hook's law, the biaxial residual stresses $\sigma_x(z)$ and $\sigma_y(z)$ at reduced thickness z (e.g. $z_0 - z$ = distance from surface) can be written as follows[22]:

$$\sigma_x(z) = \frac{E}{6(1-\nu^2)}\left[z^2\frac{d\,(P_x + \nu P_y)}{dz} + 4z\,(P_x + \nu P_y) - 2\int_z^{z_0}(P_x + \nu P_y)\,dz\right] \quad (2a)$$

$$\sigma_y(z) = \frac{E}{6(1-\nu^2)}\left[z^2\frac{d\,(P_y + \nu P_x)}{dz} + 4z\,(P_y + \nu P_x) - 2\int_z^{z_0}(P_y + \nu P_x)\,dz\right] \quad (2b)$$

E and ν are the Young's modulus (measured ~ 60 GPa) and Poisson's ratio (~ 0.25 [4]), z_0 is the starting thickness of the laminate and $P_{x,y}$, ($P = 2\varepsilon/z$) is the curvature in the x or y direction, respectively (for isotropic behaviour of square samples $P_x = P_y$ and $\sigma_x = \sigma_y$). Equation (2) was solved by numerical integration and differentiation of the experimentally determined function ($P + \nu P$) versus z with data analysis software (Origin 7.5G, OriginLab Corporation, Northampton, USA).

III. Results

(1) Sintering and thermal expansion

Monolithic laminates of both specimen sets A and B started to sinter at about 850 °C and attained a maximum sintering rate at 1150 °C. The pronounced drop in sintering strain rate at temperatures higher than 1200 (B) and 1300 °C (A), respectively, must be attributed to the allotropic β-α TCP transformation which is associated with a pronounced molar volume expansion of 7.24 % (density β-TCP 3.07 g/cm^3, α-TCP 2.86 g/cm^3 [23]). Thus, in order to avoid extended microcrack formation [24], the sintering temperature of monolithic A, B as well as sandwich A-B-A laminate specimens was limited to 1150 °C. SEM analysis confirmed that the specimens sintered at 1150 °C did not show visible microcrack formation, Fig. 2. However, residual pores distributed uniformly can still be observed and the fractional density was limited to approximately 0.95.

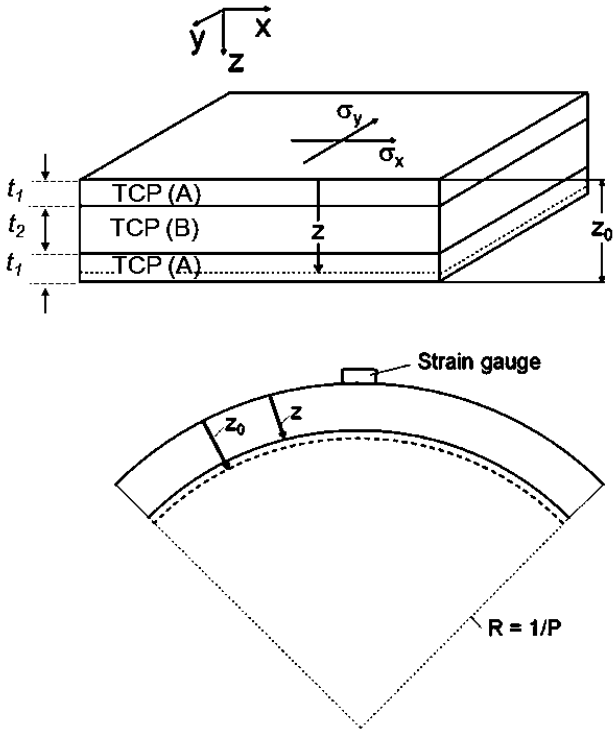

Fig. 1: Principle of the mechanical strain gauge procedure.

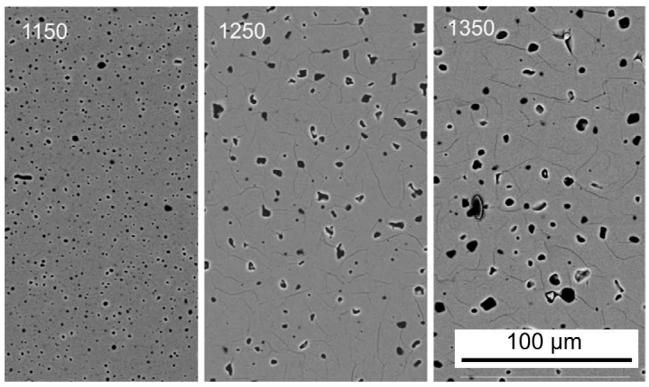

Fig. 2: Microstructure (SEM) of TCP A sintered at 1150 °C, 1250 °C, and 1350 °C showing extended microcracking induced by β-to α phase transformation at the higher sintering temperature.

Fig. 3 shows the curve of thermal expansion difference ($\Delta\alpha(T) = \alpha_B(T) - \alpha_A(T)$) as derived from dilatometric measurements of the thermal expansion of the monolithic laminates A and B. Except for the temperature interval at 700 – 1000 °C, powder B laminates exhibit a significantly larger α than powder A laminates. For the temperature interval from 1050 °C to 20 °C mean values of $\alpha_A = 12.7$ ppm/K and $\alpha_B = 14.43$ ppm/K were derived. In order to generate thermal mismatch compressive stresses on the surface of the symmetric sandwich laminates, A tapes with the lower α were selected as the outer layers and B tapes for the core layers [25].

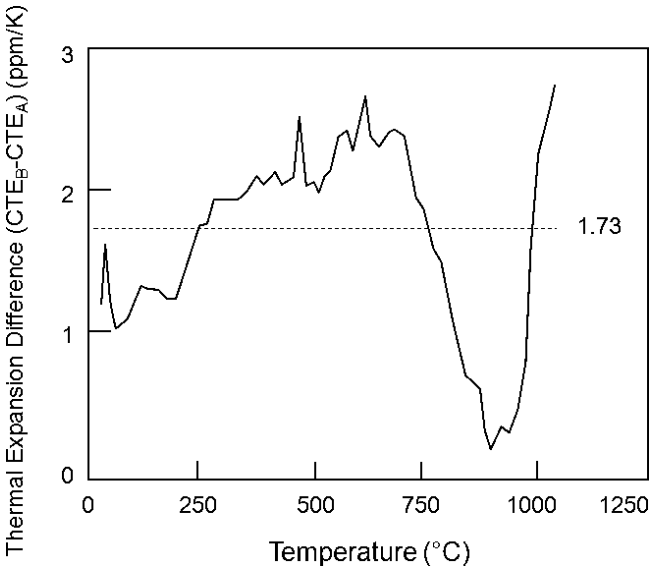

Fig. 3 : Difference in thermal expansion of sintered A and B monoliths $\Delta\alpha(T) = \alpha_B - \alpha_A$.

Despite the differences in thermal expansion, no delamination cracks could be observed at the interface between the A and B tapes in the A-B-A sandwich laminates sintered at 1150 °C, Fig. 4. Thus, it may be concluded that strong interfaces have developed which are able to avoid edge cracking owing to compression stresses localized on the surface layer [26].

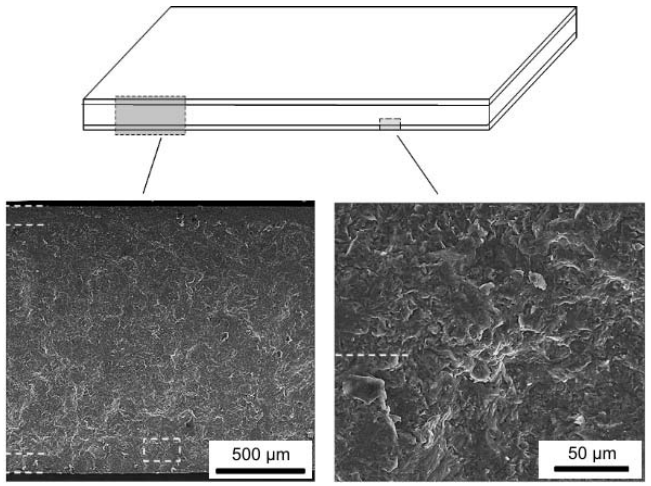

Fig. 4: Micrographs of cross-sections perpendicular to layer stacking of A-B-A sandwich laminate specimen sintered at 1150 °C.

(2) Residual stresses and strength

Near to the surface, a maximum compression stress (two-dimensional) of approximately 10 MPa was derived from the curvature measurements. The compression stress is relieved within a depth of approximately 100 µm (corresponding to the thickness of the A surface layer) and converted to a low tensile stress of a few MPa in the core region, Fig. 5.

The modulus of rupture of the monolithic specimens A and B sintered at 1150 °C attained values of 98 ± 15 MPa and 96 ± 12 MPa, respectively. At the same level of fractional density, the sandwich A-B-A laminate achieved a higher fracture stress of 113 ± 11 MPa, Fig. 6.

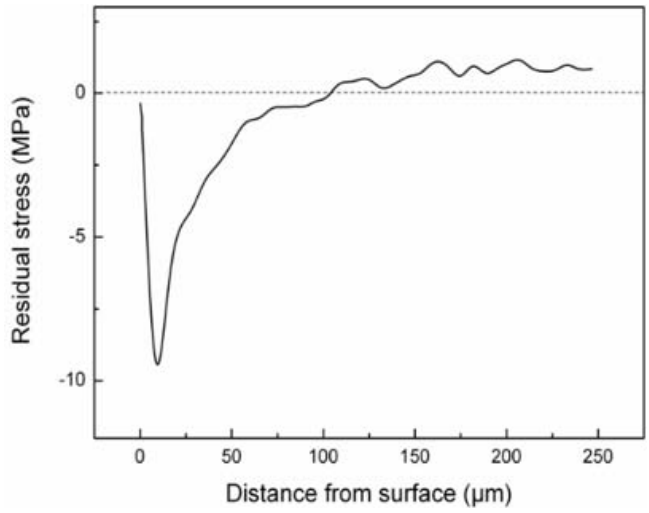

Fig. 5: Residual stress profile of A-B-A sandwich laminate measured with the strain relaxation method.

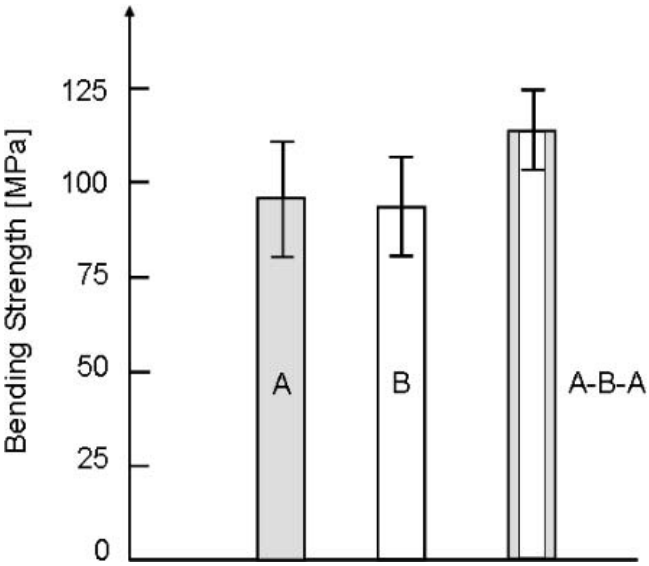

Fig. 6: Bending strength of the monolithic and sandwich-type laminates measured with the concentric ring-on-ring test.

IV. Discussion

Although the strength increment of ~ + 13 – 20 % is still relatively small, it may be attributed to the presence of compression stresses in the outer A surface layers. Evaluation of the potential stress generation may be based on plane stress analysis of the residual stresses in a symmetric three-layer composite with planar interfaces [11]

Surface:

$$\sigma_1 = - \frac{\Delta\alpha\Delta T E_1 t_2}{2t_1 (1 - \nu_2) \frac{E_1}{E_2} + t_2 (1 - \nu_1)} \qquad (3a)$$

Core:

$$\sigma_2 = - \frac{2\Delta\alpha\Delta T E_1 t_1}{2t_1 (1 - \nu_2) \frac{E_1}{E_2} + t_2 (1 - \nu_1)} \qquad (3b)$$

E_i and t_i are the Young's moduli and thicknesses of 1 (outer A-layers 0.09 mm) and 2 (core B-layers 1.9 mm), and ν_1 is the Poisson's number (0.27). Taking to a first approximation $E_1 = E_2 \approx 20$ GPa, and $\nu_1 = \nu_2 \approx 0.27$ and inserting $\Delta\alpha \approx 1.73$ ppm/K, values of residual surface compression stresses of 35 – 50 MPa are calculated for $\Delta T =$

700 – 1000 °C, which are compensated by averaged tensile stresses of 3 – 5 MPa in the core layers. Although the calculation neglects effects of layer geometry on non-uniform stress distribution, the estimated values may indicate upper limits of the residual stresses attainable with the given material constants. The discrepancies between the lower measured and the higher calculated values might be explained by stress relaxation triggered by microcrack formation. Even though extended microcracks were not visible in SEM analysis, it cannot be excluded that small fractions of α phase may have formed during sintering which have been reported to have a significant influence on the physical properties of sintered β-TCP [23]. As a consequence, stabilization of β-TCP to avoid β to α transformation as well as a reduction of residual porosity to increase the Young's modulus is a great challenge in order to achieve higher residual compression stresses on the surface of pressureless-sintered TCP ceramics. The maximum values for the Young's modulus reported for hot-pressed polycrystalline β-TCP [27] are about 50 % of the modulus of β-single crystal (nanoindentation measurement 120 GPa [28] and *ab initio* calculation 110 GPa [29]) whereas our values were 16 % only. Thus, surface compression stresses 3 – 5 times higher than the measured values should be possible by optimizing processing and consolidation.

Substitution of metal ions like Mg^{2+} on the Ca^{2+} site [18] and adding $Ca_2P_2O_7$ as a sintering aid [30] were successfully demonstrated to allow sintering temperatures exceeding 1200 °C without triggering the β to α phase transformation. Furthermore, the presence of Mg^{2+} ions in the TCP lattice inhibits grain growth during sintering [31]. The microcracking associated with the expansion-contraction cycle induced by allotropic β to α phase transformation was found to be shifted to temperatures higher than the transformation temperature when the grain size is very small [32]. Thus, microstructure refinement will not only reduce the susceptibility of this material to transformation-induced microcracking, but will also improve the densification kinetics, allowing β-TCP to be sintered to the higher densities required for generation of enhanced residual stresses on the surface of a multilayer implant device. Furthermore, previous experimental results suggested a clear effect of Mg^{2+} doping on the thermal expansion of β-TCP with α of β-TCP doped with 4.5 wt% Mg^{2+} decreasing by more than 30 % compared to Mg^{2+} free β-TCP [23]. Thus, enlarging the difference of thermal expansion between the surface layer and the core materials may be achieved by optimizing the crystal chemistry doping.

Although the experimentally measured compressive stress level and the effect on strength of pressureless-sintered β-TCP laminate ceramics is still relatively small, residual stress generation may offer interesting potential for improving strength (and toughness) of calcium phosphate bioceramics. Caution must be exercised with laminate devices when the applied (tensile) loading stresses are not confined to the surface regions but superimpose the tensile stresses in the core region of the laminate [11]. Owing to the limited strength of β-TCP (bending strength ~ 140 MPa at a fractional density of 0.99 [33]) either the surface-to-core thickness ratio (t_1/t_2) must be very small or the compression surface stress must be limited to tolerable levels in order to avoid external application load causing core fracture. To summarize, resorbable TCP implant devices capable of carrying load temporarily owing to superior mechanical properties appear to be of particular interest for a variety of applications in orthopaedic and traumatic surgery including, for example, maxillofacial augmentations or osteosynthesis.

V. Conclusions

Residual compressive stresses were generated on the surface of pressureless-sintered multilayer TCP ceramics with a symmetrical sandwich design. Compared to monolithic laminates, the sandwich laminate attained higher two-dimensional bending strength, which was attributed to the compressed surface. Optimizing processing and consolidation in order to increase Young's modulus as well as increasing the difference of thermal expansion between the surface layer and the core materials by controlled crystal chemistry doping were discussed for achieving higher compressive stresses. Enhancement of the residual stress formation is expected to offer interesting potential for improving the poor mechanical properties of β-TCP implant materials, which might then be applied even under load-bearing conditions.

Acknowledgements

Financial support from DFG project GR 961/28 is gratefully acknowledged. The authors would also like to thank Heike Reinfelder for assistance with the experiments.

References

1 LeGeros, R.Z.: Properties of Osteoconductive Biomaterials: Calcium Phosphates, *Clin. Orthop. Relat. R.*, **395**, 81, (2002).

2 Doremus, R.H.: Bioceramics, *J. Mater. Sci.*, **27**, 285 – 297, (1992).

3 LeGeros, R.Z., Lin, S., Rohanizadeh, R., Mijares, D., LeGeros, J.P.: Biphasic calcium phosphate bioceramics: preparation, properties and applications, *J. Mat. Sci. Mater. M.,* **14,** 201 – 209, (2007).

4 Metsger, D.S., Rieger, M.R., Foreman, D.W.: Mechanical properties of sintered hydroxyapatite and tricalcium phosphate ceramics, *J. Mater. Sci.-Mater M.*, **10**, 9 – 17, (1999).

5 Kaili Lin, L., Chang, J., Lu, J., Wu, W., Zeng, Y.: Properties of β-$Ca_3(PO_4)_2$ bioceramics prepared using nano-size powders, *Ceram. Int.*, **33,** 979 – 985, (2007).

6 Yu, X.Z., Cai, S., Zhang, Z., Guohua, X.: Bioactive pyrophosphate glass/beta-tricalcium phosphate composite with high mechanical properties, *Mat. Sci. Eng. C*, **28**, 1138 – 1143, (2008).

7 Mazaheri, M., Haghighatzadeh, M., Zahedi, A.M., Sadrnezhaad, S.K.: Effect of a novel sintering process on mechanical properties of hydroxyapatite ceramics, *J. Alloy. Compd.*, **471**, 180 – 184, (2009).

8 Dorozhkin, V.S.: Calcium orthophosphate-based biocomposites and hybrid biomaterials, *J. Mater. Sci.*, **44**, 2343 – 2387, (2009).

9 Selsing, J.: Internal stresses in ceramics, *J. Am. Ceram. Soc.*, **44,** 419, (1961).

10 Green, D.J.: A Technique for Introducing Surface Compression Stresses into Zirconia Ceramics, *J. Am. Ceram. Soc.*, **66,** 178 – 179, (1983).

[11] Lakshminarayanan, R., Shetty, D.K., Cutler, R.A.: Toughening of Layered Ceramic Composites with Residual Surface Compression, *J. Am. Ceram. Soc.*, **79**, 79 – 87, (1996).

[12] Green, D.J., Cai, P.Z., Messing, G.L: Residual Stresses in Alumina-Zirconia Laminates, *J. Eur. Ceram. Soc.*, **19**, 2511 – 2517, (1999).

[13] Orlovskaya, N.A., Kuebler, J, Subotin, V.I., Lugovy, M.: High Toughness Ceramic Laminates by Design of Residual Stresses, *Mater. Res. Soc. Symp. P.*, **702**, U8.7.1-U8.7.6, (2002).

[14] Tsui, Y.C., Doyle, C., Clyne, T.W.: Plasma sprayed hydroxyapatite coatings on titanium substrates Part 1: Mechanical properties and residual stress levels, *Biomaterials*, **19**, 2015 – 2029, (1998).

[15] Yang Y.C., Chang, E.: Influence of residual stress on bonding strength and fracture of plasma-sprayed hydroxyapatite coatings on Ti-6Al-4V substrate, *Biomaterials*, **22,** 1827 – 1836, (2001).

[16] Zhang, S., Wang, Y.S., Zeng, X.T., Cheng, K., Qian, M., Sun, D.E., Weng, W.J., Chia, W.Y.: Evaluation of interfacial shear strength and residual stress of sol-gel derived fluoridated hydroxyapatite coatings on Ti6Al4V substrates, *Eng. Fract. Mech.*, **74**, 1884 – 1893, (2007).

[17] Han, Y., Xu, K., Lu, J.: Dissolution response of hydroxyapatite coatings to residual stress, *J. Biomed. Mater. Res.*, **55**, 596 – 602, (2001).

[18] Enderle, R., Götz-Neunhoeffer, F., Göbbels, M., Müller, F.A., Greil, P.: Influence of magnesium doping on the phase transformation temperature of β-TCP ceramics examined by Rietveld refinement, *Biomaterials*, **26,** 3379 – 3384, (2005).

[19] Schindler, K., Roosen, A.: Manufacture of 3D structures by cold low pressure lamination of ceramic green tapes, *J. Eur. Ceram. Soc.*, **29,** 899 – 904, (2009).

[20] Soltesz, U., Richter, H., Kienzler, R.: The concentric-ring test and its application for determining the surface strength of ceramics, *Mater. Sci. Monog. (Ceram.Clin.Appl.)*, **39**, 49 – 158, (1987).

[21] Grellner, F., Höscheler, S., Greil, P., Sindel, J., Petschelt, A.: Residual stress measurements of computer aided design/computer aided manufacturing (CAD/CAM) machined dental ceramics, *J. Mater. Sci.,* **32**, 6235 – 6242, (1997).

[22] Peiter, A.: Residual Stresses of the 1st Kind – Determination and Assessment, Michael Triltsch Verlag, Düsseldorf, Germany (1966).

[23] Marchi, J., Dantas, A.C.S., Greil, P., Bressiani, J.C., Bressiani, A.H.A., Müller, F.A.: Influence of Mg-substitution on the physicochemical properties of calcium phosphate powders, *Mater. Res. Bull.*, **42**, 1040 – 1050, (2007).

[24] Cai, P.Z., Green, D.J., Messing, G.L.: Constrained Densification of Alumina/Zirconia Hybrid Laminates I: Experimental Observations of Processing Defects, *J. Am. Ceram. Soc.*, **80,** 1929 – 1939, (1997).

[25] Oel, H.J., Frechette, V.D.: Stress distribution in multiphase systems: I Composites with planar interfaces, *J. Am. Ceram. Soc.*, **50,** 542 – 549, (1967).

[26] Bermejo, R., Danzer, R.: Failure Resistance Optimisation in Layered Ceramics Designed with Strong Interfaces, *J. Cer. Sci. Tech.*, **1,** 15 – 20, (2010).

[27] Wang, C.X., Zhou, X., Wang, M.: Influence of sintering temperatures on hardness and Young's modulus of tricalcium phosphate bioceramic by nanoindentation technique, *Mater. Charact.*, **52**, 301 – 307, (2004).

[28] Viswanath, B., Raghavan, R., Gurao, N.P, Ramamurty, U., Ravishankar, N.: Mechanical properties of tricalcium phosphate single crystals grown by molten salt synthesis, *Acta Biomater.*, **4**, 1448 – 1454, (2008).

[29] Liang, L., Rulis, P., Ching, W.Y.: Mechanical properties, electronic structure and bonding of α-and β-tricalcium phosphates with surface characterization, *Acta Biomater.,* **6**, 3763 – 3771, (2010).

[30] Ryu, H.S., Youn, H.J., Hong, K.S., Chang, B.S., Lee, C.K., Chung, S.S., An improvement in sintering property of beta-tricalcium phosphate by addition of calcium pyrophosphate, *Biomaterials*, **23,** 909 – 914, (2002).

[31] Itatani, K., Takahashi, M., Howell, F.S., Aizawa, M.: Effect of metal-oxide addition on the sintering of β-calcium orthophosphate, *J. Mater. Sci.: Mater. M.*, **13**, 707 – 713, (2002).

[32] Perera, F.H., Martinez-Vazquez, F.J., Miranda, P., Ortiz, A.L., Pajares, A.: Clarifying the effect of sintering conditions on the microstructure and mechanical properties of β-tricalcium phosphate, *Ceram. Int.,* **36**, 1929 – 1935, (2010).

[33] Akao, M., Aoki, H., Kato, K., Sato, A.: Dense polycrystalline β-tricalcium phosphate for prosthetic applications, *J. Mat. Sci.*, **17**, 343 – 346, (1982).